Available online at www.sciencedirect.com

ScienceDirect

IFAC Papers Online CONFERENCE PAPER ARCHIVE

IFAC-PapersOnLine 49-12 (2016) 967–972

Design of experiments for elastostatic calibration of heavy industrial robots with kinematic parallelogram and gravity compensator

A. Klimchik*, E. Magid*, A. Pashkevich**

* Innopolis University, Universitetskaya 1, 420500 Innopolis, The Republic of Tatarstan, Russia (e-mail: a.klimchik@innopolis.ru, e.magid@ innopolis.ru)

** Ecole des Mines de Nantes, 4 rue Alfred-Kastler, Nantes 44307, France (e-mail: anatol.pashkevich@mines-nantes.fr)

Abstract: The paper deals with elastostatic calibration of quasi-serial heavy robots with kinematic parallelograms and gravity compensators. Particular attention is paid to the selection of optimal measurement configurations allowing to reduce the measurement noise impact on the identification accuracy. For these types of manipulators, the identification equations are highly non-linear with respect to the parameters to be calibrated. For this specific architecture, a two-steps identification procedure is developed and a new technique of the calibration experiment design is proposed, which allows improving the identification accuracy without increasing the number of measurements. The developed technique is illustrated by an application example that deals with a typical heavy quasi-serial industrial robot.

Keywords: industrial robot, stiffness modeling, calibration, gravity compensator, design of experiments.

1. INTRODUCTION

At present, industrial robots progressively replace CNC-machines in different technological processes including machining of large-dimensional parts for aerospace and shipbuilding industries. However, this replacement requires essential efforts in improving robot accuracy under external loading that is often not high enough and strongly depends on the control strategy. For the tasks where high precision is unimportant, the conventional control strategy based on the geometric model is sufficient and allows user to achieve the desired performance. If the accuracy becomes a critical issue and the robot is subject to essential external loadings, the control strategy should take into account the manipulator elasticity (Klimchik et al., 2013a, Chen et al., 2013). The latter requires a reliable stiffness model that can be used for compensation of the compliance errors caused by the tool-workpiece interaction and influence of the gravity forces (Abele et al., 2012).

In literature, there exist different stiffness modeling approaches that can be used for robotic manipulators. The most convenient of them is the Virtual Joint Modeling method (VJM), which extends a traditional rigid body model by adding virtual springs describing the manipulator compliance (Pashkevich et al., 2011). Recent advances in this area allows user to describe link/joint elasticity by sophisticated 6 dof springs, to take into account impact of different types of loadings (Klimchik et al., 2014a). This approach can be efficiently applied to for fully actuated or under-actuated, over-constrained and under-constrained architectures (Quennouelle and Gosselin, 2008, Kövecses and Angeles, 2007, Ceccarelli and Carbone, 2002). However, existing techniques implicitly assume that manipulator is either strictly serial or strictly parallel. For this reason, for the manipulators with internal loops induced by mechanical components the general methodology should be revised.

It should be noted that stiffness modeling for quasi-serial manipulators is quite a new problem in robotics that was not studied in details before. Its importance progressively increases since a number of recent industrial robots include internal closed-loops formed by gravity compensators or/and kinematic parallelograms (Fig. 1). One of the pioneer works in this direction is devoted to replacing the kinematic parallelogram by an equivalent virtual spring (Pashkevich et al., 2010), which allows to apply conventional stiffness modeling technique developed for serial manipulators. However, the obtained results cover the passive parallelogram cases only, while the widely used in heavy industrial robots active parallelogram cases (Fig. 1b) are outside of the scope of existing works. Another important issue in this area is related to the stiffness modeling of industrial robots with spring-based gravity compensators (Klimchik et al., 2013b). For such mechanisms, there are quite limited number of works that deal with particular cases (Klimchik et al., 2012).

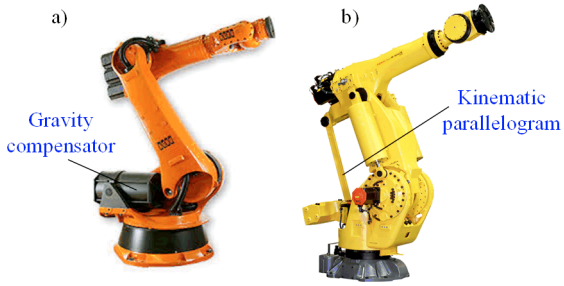

Fig. 1. Examples of quasi-serial robots with internal loops

For quasi-serial manipulators, the problem of elastostatic parameters identification is essentially harder compared to serial or parallel ones (Alici and Shirinzadeh, 2005, Meggiolaro et al., 2005). For this reason, none of the existing techniques can be applied directly. Besides, proper selection

10.1016/j.ifacol.2016.07.901

of measurement configurations is a non-trivial task here, since the related optimization problem should be solved for two mutually dependent sets of variables. This problem has never been studied in the literate before but deserves special attention.

2. PROBLEM STATEMENT

Let us consider a quasi-serial manipulator with internal loops, created by a kinematic parallelogram and/or a gravity compensator. Typical architecture of such robot is presented in Fig. 1. Relevant elasto-static model of the considered robot can be obtained using the VJM-technique, which leads to a quasi-rigid structure composed of a number of rigid links, perfect actuated joints, perfect passive joins and a set of virtual springs describing manipulator compliance (Fig. 2).

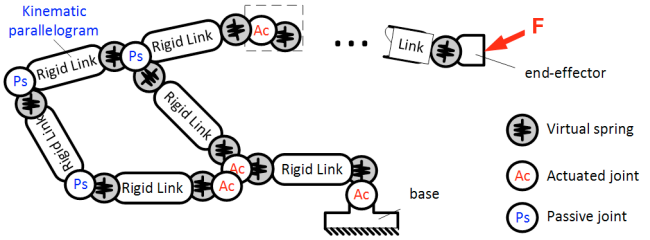

Fig. 2. VJM-based stiffness model of a quasi-serial robot.

For the *strictly serial* manipulator, the VJM-based stiffness model is presented in the following way

$$\Delta\mathbf{t} = \sum_{i=1}^{n}\left(\mathbf{J}_\theta^{(i)}\mathbf{k}_\theta^{(i)}\mathbf{J}_\theta^{(i)\mathrm{T}}\right)\cdot\mathbf{W} \tag{1}$$

where $\Delta\mathbf{t}$ is the end-effector deflection (position and orientation) caused by the external wrench $\mathbf{W}$, the matrices $\mathbf{k}_\theta^{(i)} = (\mathbf{K}_\theta^{(i)})^{-1}$ are the link/joint compliances to be identified, $\mathbf{J}_\theta^{(i)}$ are corresponding Jacobians, and n is the virtual springs number. In this case, the force-deflection relation in the joint space is linear and does not depend on the manipulator configuration. So, it is possible to apply the classical least square identification technique with the objective function

$$\sum_{j=1}^{m}\left\|\Delta\mathbf{p}_j - \left[\sum_{i=1}^{n}\left(\mathbf{J}_\theta^{(i,j)}\mathbf{k}_\theta^{(i)}\mathbf{J}_\theta^{(i,j)\mathrm{T}}\right)\cdot\mathbf{W}_j\right]^{(p)}\right\|^2 \to \min_{\mathbf{k}} \tag{2}$$

which evaluates the difference between the measured and computed position deflections. Here, $[.]^{(p)}$ denotes the position component of the full-scale deflection vector $\Delta\mathbf{t}$, m is the number of measurements. It can be proved that in this case the desired parameters can be found using expression

$$\mathbf{k} = \left(\sum_{j=1}^{m}\mathbf{A}_j^{(p)^T}\mathbf{A}_j^{(p)}\right)^{-1}\cdot\left(\sum_{j=1}^{m}\mathbf{A}_j^{(p)^T}\Delta\mathbf{p}_j\right) \tag{3}$$

where $\mathbf{k} = col\left(\mathbf{k}_\theta^{(1)},\mathbf{k}_\theta^{(2)},...\right)$ is the vector of the joint compliances, $\Delta\mathbf{p}_j$ is the vector of measured end-effector deflections in the ith experiment, $\mathbf{A}_j^{(p)}$ are the positional components of the observation matrices $\mathbf{A}_j$ (Klimchik et al., 2014b). These matrices are expressed via the Jacobian column $\mathbf{J}_1^{(j)},\mathbf{J}_2^{(j)},...,\mathbf{J}_n^{(j)}$ as

$$\mathbf{A}_j = \left[\mathbf{J}_1^{(j)}\mathbf{J}_1^{(j)^T}\mathbf{W}_j,...,\mathbf{J}_n^{(j)}\mathbf{J}_n^{(j)^T}\mathbf{W}_j\right] \quad (j=\overline{1,m}) \tag{4}$$

To apply similar technique for the *quasi-serial* manipulator, the VJM-based stiffness model should be modified by selection of a principal serial chain and introducing the configuration-dependent joint stiffness matrices. This yields the following force-deflection relation

$$\Delta\mathbf{t}_j = \sum_{i=1}^{n}\left(\mathbf{J}_\theta^{(i,j)}\mathbf{k}_\theta^{(i)}(\mathbf{q}_j)\mathbf{J}_\theta^{(i,j)\mathrm{T}}\right)\cdot\mathbf{W}_j \tag{5}$$

that cannot be treated in the usual way and requires additional efforts for parameters identification. An efficient approach has been presented in our previous work (Klimchik et al., 2013b), where the force-deflection relation was linearized for certain sub-sets of $\mathbf{q}$ and the two-steps identification procedure was used. In spite of the fact that this approach is quite general, it requires proper selection of these sub-sets for each particular case.

Besides, there is another important problem targeted at minimization of the measurement noise impact. It deals with selection of optimal measurement configurations allowing to identify the desired parameters with the highest possible precision. Mathematically, it corresponds to the minimization of the covariance derived from the optimization problem

$$\sum_{j=1}^{m}\left\|\Delta\mathbf{p}_j^0 + \boldsymbol{\varepsilon}_j - \left[\sum_{i=1}^{n}\left(\mathbf{J}_\theta^{(i,j)}\mathbf{k}_\theta^{(i)}(\mathbf{q}_j)\mathbf{J}_\theta^{(i,j)\mathrm{T}}\right)\cdot\mathbf{W}_j\right]^{(p)}\right\|^2 \to \min_{\mathbf{k}} \tag{6}$$

which includes random measurement errors $\boldsymbol{\varepsilon}_j$ that corrupt true values of the end-effector deflections $\Delta\mathbf{p}_j^0$.

To address the above problems the paper focuses on the following tasks: (i) obtaining of the VJM-based stiffness model for the quasi-serial manipulator with a kinematic parallelogram and/or a gravity compensator; (ii) developing of a methodology for identification of manipulator elastic parameters; (iii) selection of optimal measurement configurations allowing to increase identification accuracy.

3. STIFFNESS MODEL OF A QUASI-SERIAL ROBOT

3.1. Manipulator architecture

Let us consider an industrial manipulator with a kinematic parallelogram and gravity compensators using example of FANUC M-900iB/700 robot (Fig. 1b). Its kinematic architecture is presented in Fig. 3. The manipulator contains an active kinematic parallelogram with three passive joints and two actuators on the same axis, a spring-based gravity compensator connected with the second actuator, and two mass-based compensators.

Comparing to the pure-serial architectures, the considered manipulator contains two closed-loops that have impact on its force-deflection behavior. In this case, to conserve the conventional VJM approach it is reasonable to introduce non-linear virtual springs in the second joint, which take into account particularities of this architecture. Relevant geometric parameters and notations are presented in Fig. 3.

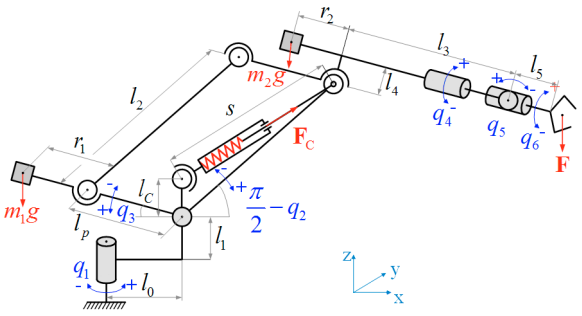

Fig. 3. Architecture of FANUC M-900iB/700 manipulator

3.2. Stiffness model of a spring-based gravity compensator

A geometric model of the spring-based gravity compensator of the robot under study is presented in Fig. 4. It contains a mechanical linear compression spring with two passive joints at the ends. The first of them is aligned with the axis #3, the second one is attached to the manipulator link #1. This mechanism creates a closed-loop generating additional torque in the second actuated joint. It is clear that this torque depends on the joint variable q_2.

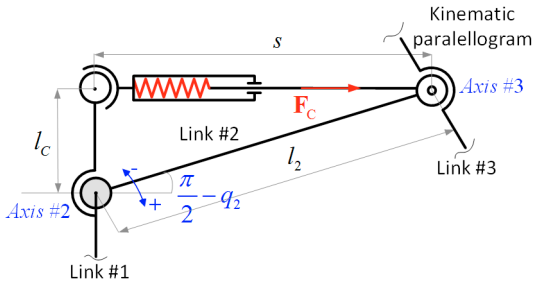

Fig. 4. Geometry of the spring-based gravity compensator

As follows from the figure, the compensator spring length s depends on q_2 and can be computed from the expression

$$s^2 = l_C^2 + l_2^2 - 2 l_C \cdot l_2 \cdot \cos q_2 \tag{7}$$

where l_C and l_2 are the compensator parameters. This allows us to express the spring compression force F_C after introducing the preloading parameter s_0 as

$$F_C = K_C \cdot (s - s_0) \tag{8}$$

where K_C is the spring stiffness constant. Further, using the law of sine one can compute the compensator torque M_C applied to the second joint

$$M_C = K_C \cdot l_C \cdot l_2 \cdot (1 - s_0 / s) \cdot \sin q_2 \tag{9}$$

and obtain the aggregated stiffness coefficient $K^{\Sigma}_{\theta_2}$ that takes into account both compensator elasticity and the second actuator compliance

$$K^{\Sigma}_{\theta_2} = K_{\theta_2} + K_C l_C l_2 \eta_{q_2} \tag{10}$$

Here K_{θ_2} is the stiffness of the second joint, η_{q_2} is a dimensionless coefficient that is computed as

$$\eta_{q_2} = \cos q_2 + \frac{s_0 l_C l_2}{s^3} \cdot \sin q_2 - \frac{s_0}{s} \cos q_2 \tag{11}$$

and depends on both the angle q_2 and the preloading s_0.

3.3. Stiffness modeling of a mass-based gravity compensator

In the manipulator under study, there are also two mass-based gravity compensators. The first of them (m_1) is located on extension of the parallelogram lower edge; it is aimed at reducing of the torque in the actuated joint #3. The second one (m_2) is located at the upper parallelogram edge; It compensates the masses of the link #3 and robot wrist. It should be stressed that the second compensator is implemented using the masses of the robot wrist actuating motors.

Both of the mass-based compensators effect the end-effector location, but they do not influence the robot response to the external loading, i.e. the force-deflection behavior. Hence, these masses should be taken into account in stiffness modeling in order to determine the end-effector displacement and the joint deflections due to the applied wrench (caused by gravity forces, internal and external loadings). However, they do not effect identification of the manipulator elastostatic parameters since their impact is the same for both loaded and unloaded cases. The difficulties here may arise only if, due to the external loading, the vertical line passing the compensator mass center intersects the parallelogram passive joint. It can be shown that in the relevant configurations the force-deflection relation is discontinuous. For this reason, it is prudent to avoid corresponding measurement configurations in calibration experiments.

3.4. Stiffness model of a kinematic parallelogram

Now, let us consider particularities of stiffness modeling for closed-loops induced by kinematic parallelograms. Typical active parallelogram with two actuators and three passive joints is presented in Fig. 5. It is assumed that the parallelogram is perfect and its geometry is defined by the parameters l_2 and l_p. The actuators drive the angles q_2, q_3 and rotate the link #2 and link #3p respectively. From geometric point of view, compared to the conventional serial architecture, such actuators location does not affect the position and orientation of the link #3, since the angle of the motor #3 is directly included in the angle q_3'. From the control point of view, driving this parallelogram-based mechanism requires recomputing of input signal for the third actuator only. Such solution improves the robot dynamics (since the heavy third motor is moved to the base to reduce inertial forces) and benefits from the elastostatic point of view as parallel chain increases the stiffness of the robot. Yet, the stiffness model of the parallelogram-based structure cannot be described similar to the conventional serial chain.

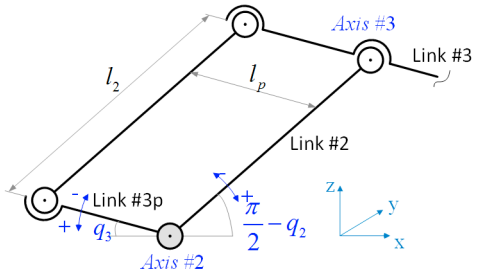

Fig. 5. Active kinematic parallelogram of industrial robots

To prove that conventional stiffness model with a 1-dof virtual spring in Axis #3 cannot describe elasto-static properties of the kinematic parallelogram, let us transform the joint compliance matrix $\mathbf{k}_P = diag(k_2, k_3)$ from a quasi-serial to an equivalent serial representation, i.e. from the space (q_2, q_3') to the space (q_2, q_3). For the parallelogram, the Jacobian matrix is presented as

$$\mathbf{J}_P = \begin{bmatrix} -l_2 \sin q_2 & -l_3 \sin q_3 \\ l_2 \cos q_2 & l_3 \cos q_3 \end{bmatrix} \tag{12}$$

For the equivalent serial chain, corresponding matrix is

$$\mathbf{J}_S = \begin{bmatrix} -l_2 \sin q_2 - l_3 \sin(q_2 + q_3) & -l_3 \sin(q_2 + q_3) \\ l_2 \cos q_2 + l_3 \cos(q_2 + q_3) & l_3 \cos(q_2 + q_3) \end{bmatrix} \tag{13}$$

Both models should lead to the same Cartesian stiffness matrix, i.e.

$$\left(\mathbf{J}_P \mathbf{k}_P \mathbf{J}_P^T\right)^{-1} = \left(\mathbf{J}_S \mathbf{k}_S \mathbf{J}_S^T\right)^{-1} \tag{14}$$

whose solution allows us to find an equivalent joint compliance matrix

$$\mathbf{k}_S = \mathbf{J}_S^{-1}\mathbf{J}_P\mathbf{k}_P\mathbf{J}_P^T\mathbf{J}_S^{-T} \tag{15}$$

After relevant substitutions of (12), (13) into (15) one can get a non-diagonal matrix

$$\mathbf{k}_S = \begin{bmatrix} k_2 & -k_3 \\ -k_3 & k_3 \end{bmatrix} \tag{16}$$

for which there is no physically meaningful counterpart in the frame of serial chain architecture.

Hence, the obtained expression (16) for equivalent serial chain proves that it is not possible to define an equivalent 1-dof virtual spring in Axis #3 that takes into account the actuator #3 compliance for the parallelogram. Nevertheless, if the user prefers the serial model, it is required to use a non-diagonal stiffness matrix in the joint space. This restriction does not violate general idea of VJM approach and can be used in certain cases. However, to simplify the model in the joint space, it is easier to take into account the particularities of parallelogram structure by modifying the Jacobian matrix.

3.5. Stiffness model of a quasi-serial robotic manipulator

VJM approach presents a serial manipulator as the sequence of rigid links separated by the actuators and virtual springs, which describe the robot elasticity (Fig. 2). For the considered types of robots, the gravity forces influence is not negligible and should be incorporated into the appropriate stiffness model. In the frame of the VJM technique, it is convenient to replace the link weights by the equivalent pair of the forces applied to the both link ends. To describe the weight of the mass-based gravity compensators, it is required to add additional nodes to the model, which correspond to their gravity centers. Then, it is possible to aggregate all weight components applied to the same virtual joint in the vectors $\mathbf{G}_i$, that can be collected in the matrix $\mathbf{G} = [\mathbf{G}_1 ... \mathbf{G}_n]$. Another loading to be considered is an external loading $\mathbf{F}$ applied to the robot end-effector.

Next, it is required to introduce the vector functions $\mathbf{g}(\mathbf{q},\boldsymbol{\theta})$ and $\mathbf{g}_j(\mathbf{q},\boldsymbol{\theta})$ defining positions of the end-effector $\mathbf{t}$ and node centers $\mathbf{t}_j$ (Klimchik et al., 2014a). These functions depend on the vectors of the actuator and virtual joint coordinates $\mathbf{q}, \boldsymbol{\theta}$. The static equilibrium equations in this case is written as

$$\mathbf{J}_\theta^{(\mathrm{G})\mathrm{T}} \cdot \mathbf{G} + \mathbf{J}_\theta^{(\mathrm{F})\mathrm{T}} \cdot \mathbf{F} = \mathbf{K}_\theta \cdot \boldsymbol{\theta} \tag{17}$$

where $\mathbf{J}_\theta^{(\mathrm{G})} = \left[\mathbf{J}_\theta^{(1)\mathrm{T}} ... \mathbf{J}_\theta^{(n)\mathrm{T}}\right]^{\mathrm{T}}$ and $\mathbf{J}_\theta^{(\mathrm{F})} = \mathbf{J}_\theta^{(n)}$ are the Jacobians computed with respect to the relevant nodes where the forces are applied to, i.e. $\mathbf{J}_\theta^{(j)} = \partial \mathbf{g}_j(\mathbf{q},\boldsymbol{\theta}) / \partial \boldsymbol{\theta}$; and matrix $\mathbf{K}_\theta$ aggregates the stiffness of all virtual springs. Here, the matrix $\mathbf{K}_\theta$ is diagonal if the joint compliance corresponding to the third motor is computed using relevant expressions. To find the desired static equilibrium, the above system should be solved subject to the geometrical constraint $\mathbf{t} = \mathbf{g}(\mathbf{q},\boldsymbol{\theta})$.

Linearization of the force-deflection relation (17) leads to the following expression for the Cartesian stiffness matrix

$$\mathbf{K}_\mathrm{C} = \left(\mathbf{J}_\theta^{(\mathrm{F})}(\mathbf{K}_\theta - \mathbf{H}_{\theta\theta})^{-1}\mathbf{J}_\theta^{(\mathrm{F})\mathrm{T}}\right)^{-1} \tag{18}$$

It worth mentioning that the above expression is valid for the case of manipulators without internal loops, where the matrix $\mathbf{K}_\theta$ is constant. To take into account the compensator influence, these expressions should be modified by using the configuration dependent joint stiffness matrix $\mathbf{K}_\theta(\mathbf{q})$ describing properties of the virtual springs.

4. ELASTOSTATIC PARAMETERS IDENTIFICATION

To take into account the compensator influence while retaining conventional approach developed for pure-serial manipulators without closed-loops, it is convenient to consider several independent parameters $k_{\theta_{2j}}$ corresponding to each different value of q_2. In this case the identification problem remains linear and can be solved using the conventional least-square technique, but the desired elastostatic parameters for the closed-loop elements (compensator stiffness and preloading and second joint compliance) will be identified on the second step.

Denoting the desired parameters set $\mathbf{k} = [k_1, (k_{21}, k_{22}..), .., k_6]$ allows us to present the identification equation in the form

$$\Delta\mathbf{p}_j = \mathbf{B}_j^{(p)}\mathbf{k} \qquad (j = \overline{1,m}) \tag{19}$$

where matrices $\mathbf{B}_j^{(p)}$ are composed of the elements of $\mathbf{A}_j^{(p)}$. More details concerning construction of $\mathbf{B}_j^{(p)}$ can be found in our previous work (Klimchik et al., 2013b).

Using the above notations, the first step of the elastostatic parameters identification leads to the following expression

$$\mathbf{k} = \left(\sum_{j=1}^{m} \mathbf{B}_j^{(p)T}\mathbf{B}_j^{(p)}\right)^{-1} \cdot \left(\sum_{j=1}^{m} \mathbf{B}_j^{(p)T}\Delta\mathbf{p}_j\right) \tag{20}$$

Further, the second step of the identification procedure should be applied. It is based on (10) and allows us to obtain parameters of the gravity compensator and the second joint

$$\begin{bmatrix} K_{\theta_2} & K_C & s_0 \cdot K_C \end{bmatrix}^T = \left(\sum_{i=1}^{m_q} \mathbf{C}_i^T\mathbf{C}_i\right)^{-1}\left(\sum_{i=1}^{m_q} \mathbf{C}_i^T K_{\theta_{2i}}\right) \tag{21}$$

where m_q is the number of q_2 in the experimental data and

$$\mathbf{C}_i = \begin{bmatrix} 1 & l_C l_2 \cos q_{2i} & l_C l_2 \left(l_C l_2 \sin q_2 / s^3 - \cos q_{2i} / s\right) \end{bmatrix} \tag{22}$$

Thus, the proposed modification of the calibration technique allowing to find the manipulator and compensator parameters sequentially. An open question, however, is how to find the set of measurement configurations that ensures the lowest impact of the measurement errors.

5. DESIGN OF CALIBRATION EXPERIMENTS

5.1. Design of experiments for the robot base orientation

The robot base orientation is defined by the first actuator and does not affect the elastostatic calibration if vertical loading is used. For this reason, it can be chosen arbitrary in order to facilitate the experiments. On the other side, it is not possible to identify compliance of the first joint using vertical force only. To overcome this difficulty, it usually required to carry out additional experiments with non-vertical loading. In this case, it is required to select measurement configurations for which deflections in Joint #1 are maximal and to have maximum distance from the joint axis to the measurement point. Hence, it is preferable here to have a robot with outstretched arm. Besides, to avoid influence of other compliant elements, the manipulator wrist should be oriented along the force direction. These practical ideas allow us to design the calibration experiments for the robot base orientation.

5.2. Design of experiments for kinematic parallelogram

Since the kinematic parallelogram includes the second and the third actuators, the calibration experiment design for the angles q_2 and q_3 cannot be separated. To evaluate the quality of measurement configurations, three different performance measures (PM) are used:

O_1: the trace of the parameter covariance matrix;

O_2: the determinant of the parameter covariance matrix;

O_3: the weighted sum of the trace and the determinant.

To take into account the workspace limitations induced by the experimental setup, let us plot x and z coordinates of wrist location as a functions of joint angles q_2 and q_3 (Fig. 6).

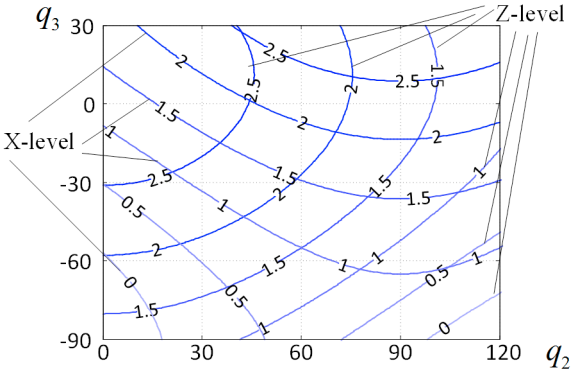

Fig. 6. Optimal set of the parallelogram angles (q_2, q_3).

Taking into account that the calibration experiments cannot be implemented for z<0.5 m and closer than 1 m from the axis #1, one can define reachable workspace. It can be shown that in our experimental setup the variation of q_2 is $[0^o..120^o]$ and q_3 variation is $[-30^o..30^o]$. The obtained optimal values for different number of measurement configurations and different performance measures are given in Table 1. As follows from the table, there is no accuracy improvement from increasing the number of different q_2. In fact, similar effect can be achieved by simple repeating of measurements for three different angles q_2.

Table 1. Optimal values of PMs

Performance measure	O_1	O_2	O_3
3 measurement configurations			
Value of PM	14.27	2.11	8.19
Value per configuration	42.81	6.33	24.57
4 measurement configurations			
PM value	9.85	1.68	5.77
Value per configuration	39.4	6.72	23.08
5 measurement configurations			
PM value	7.86	1.33	4.59
Value per configuration	39.3	6.65	22.95

To select angles q_2, the following technique can be applied that follows from the simulation analysis. First, it is reasonable to choose two values of q_2 corresponding to the joint limits (i.e. 0° and 120°). Then, it is necessary to find the third angle, which varied from 47.1° to 50.0° depending on PM. As follows from the dedicated study presented in Fig. 7, the sensitivities of PMs is rather low in this range. Admissible ranges of the third value of q_2 for different PMs are summarized in Table 2.

Table 2. Ranges of q_2 for different accuracy levels

lose of accuracy	Angle range , deg (value of PM)		
	O_1	O_2	O_3
min	50 (2.11)	47 (14.3)	47 (8.2)
10% interval	33..68 (2.32)	37..57 (15.7)	38..57 (9.0)
20% interval	26..75 (2.53)	35..60 (17.1)	34..61 (9.8)
50% interval	17..87 (3.16)	29..67 (21.4)	23..75 (16.3)

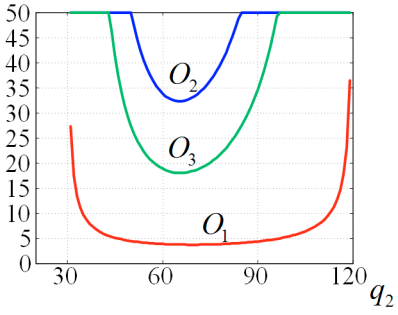

Fig. 7. Sensitivity of PMs with respect to q_2 (middle value)

As follows from the Table 2, with the 10% loss of accuracy it is possible to choose the middle angle in the interval 38°..57° and with 20% lose this interval increases up to 34°..60°. This gives us some freedom to select the third value of q_2 without essential impact on the identification accuracy. Below, final selection of this angle will be done after considering the noise impact on the identification accuracy of the aggregated parameters.

For the angle q_3, the design of experiments is similar to the linear case. It follows from the fact that the mass-based gravity compensators do not influence on the manipulator reaction to the external loading. For such problems, the design of experiment theory suggests taking measurements on the both sides of the workspace. Thus, taking into account the experimental setup limits, fixing angles q_3 to 30° and -30° will ensure maximum variation range for q_2 angle.

Hence, the obtained optimal plan of calibration experiments for the manipulator parallelogram includes three different angles q_2 and two angles q_3. This corresponds to six measurement configurations that ensure sufficient rank of the observation matrix. For this plan, the measurement points are located in the joint space corners and also in an intermediate point for q_2. To choose the intermediate value of q_2, let us evaluate influence of measurement noise on the identification accuracy of the aggregated model parameters. Relevant study was done for different values of middle point q_2 while fixing remaining values of q_2, q_3 on the borderers. Table 3 summarizes the simulation results and shows identification accuracy of all aggregated parameters (i.e. their variance) for different middle angle q_2 obtained by means of minimization of the diagonal elements of the covariance matrix.

Table 3. Impact of middle angle q_2 on the identification accuracy of aggregated parameters

q_2 optimal	Identification accuracy for aggregated parameters, Nm/μrad				
	$q_2 = 0$	$q_2 = 120$	q_2=vary	$q_3 = -30$	$q_3 = 30$
88°	0.66	1.22	2.00	0.48	0.45
67°	0.66	1.22	1.54	0.47	0.47
2°	0.71	1.25	0.71	0.55	0.50
67°	0.66	1.22	1.54	0.47	0.47
112°	0.67	1.23	1.62	0.50	0.44

Table 4. Accuracy levels for aggregated parameters

lose of accuracy	Angle range , deg (value of PM)					Parameters accuracy range
	q_2=0°	q_2= 120°	q2=vary	q_3=-30°	q_3=30°	
min	88	67	2	67	112	47..50
	0.66	1.22	0.71	0.47	0.44	
10%	0..120	0..120	0..32	20..120	53..120	38..57
interval	0.73	1.34	0.78	0.52	0.48	
20%	0..120	0..120	**0..40**	0..120	0..120	35..60
interval	0.79	(1.46)	(0.85)	0.56	0.53	
50%	0..120	0..120	0..54	0..120	0..120	29..67
interval	0.99	1.83	1.06	0.71	0.66	

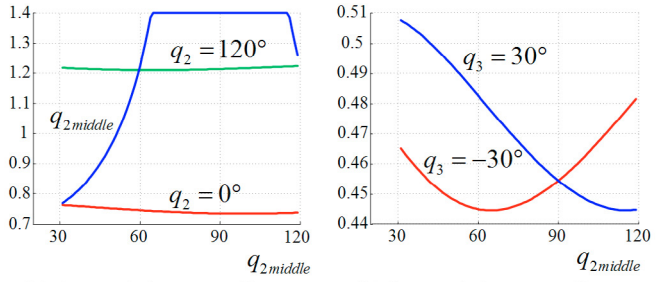

(a) Aggregated accuracy for q_2 (b) Aggregated accuracy for q_3

Fig. 8. Identification accuracy for aggregated parameters

As follows from the above table, the identification accuracy for the aggregated parameters corresponding to q_2=0° and q_2=120° do not vary essentially with changing the intermediate value of q_2. From the other side, the accuracy of the third aggregated parameter highly depends on the choice of the middle value of q_2. (Fig. 8a). The identification accuracy of the forth and fifths parameters depends on the middle value of q_2,, but it varies by 20% only (Fig. 8b). Using these data, the accuracy levels for all desired parameters were defined and are presented Table 4.

As follows from the presented results, the range of 35°..40° of the middle value of q_2 gives a reasonable trade-off for all desired parameters. For this reason, it was assigned to 35°.

5.3. Optimal selection of the wrist configurations

Similar to the parallelogram case, the optimal wrist configurations were obtained via numerical optimization of the performance measures O_1, O_2, and O_3. It should be mentioned that the obtained solutions are in a good agreement with analytical rules proposed in our previous work (Klimchik et al., 2015). The full set of measurement configurations is given in Table 5.

Table 5. Optimal measurement configurations for elastostatic calibration of robot Fanuc M-900iB/700

q_1	q_2	q_3	q_4	q_5	q_6
0	0	-30	-45	30	135
0	0	-30	45	-30	35
90	0	30	-45	-30	-45
90	0	30	45	-30	45
180	35	-30	135	-30	-45
-180	35	-30	-45	30	135
-90	35	30	135	30	135
-90	35	30	-45	-30	-45
0	120	-30	-135	30	-135
0	120	-30	135	-30	-45
180	120	30	-135	30	-135
-180	120	30	135	30	135

6. CONCLUSIONS

The paper focuses on the stiffness modeling of quasi-serial industrial robots with active kinematic parallelograms and gravity compensators. It proposes a new technique of calibration experiment design, which essentially reducing the measurement noise impact on the parameters identification accuracy. The advantages of the developed techniques are illustrated by an experimental case study that deals with the quasi-serial industrial robot Fanuc M-900iB/700. In future, the obtained results will be applied to a larger set of industrial robots.

ACKNOWLEDGMENT

The work presented in this paper was partially funded by the project FEDER ROBOTEX, France.

REFERENCES

ABELE, E., SCHÜTZER, K., BAUER, J. & PISCHAN, M. 2012. Tool path adaption based on optical measurement data for milling with industrial robots. *Production Engineering,* 6**,** 459-465.

ALICI, G. & SHIRINZADEH, B. 2005. Enhanced stiffness modeling, identification and characterization for robot manipulators. *Robotics, IEEE Transactions on,* 21**,** 554-564.

CECCARELLI, M. & CARBONE, G. 2002. A stiffness analysis for CaPaMan (Cassino parallel manipulator). *Mechanism and Machine Theory,* 37**,** 427-439.

CHEN, Y., GAO, J., DENG, H., ZHENG, D., CHEN, X. & KELLY, R. 2013. Spatial statistical analysis and compensation of machining errors for complex surfaces. *Precision Engineering,* 37**,** 203-212.

KLIMCHIK, A., CARO, S. & PASHKEVICH, A. 2015. Optimal pose selection for calibration of planar anthropomorphic manipulators. *Precision Engineering,* 40**,** 214-229.

KLIMCHIK, A., CHABLAT, D. & PASHKEVICH, A. 2014a. Stiffness modeling for perfect and non-perfect parallel manipulators under internal and external loadings. *Mechanism and Machine Theory,* 79**,** 1-28.

KLIMCHIK, A., PASHKEVICH, A., CHABLAT, D. & HOVLAND, G. 2013a. Compliance error compensation technique for parallel robots composed of non-perfect serial chains. *Robotics and Computer-Integrated Manufacturing,* 29**,** 385-393.

KLIMCHIK, A., PASHKEVICH, A., WU, Y., CARO, S. & FURET, B. 2012. Design of calibration experiments for identification of manipulator elastostatic parameters. *Applied Mechanics and Materials,* 162**,** 161-170.

KLIMCHIK, A., WU, Y., CARO, S., FURET, B. & PASHKEVICH, A. 2014b. Geometric and elastostatic calibration of robotic manipulator using partial pose measurements. *Advanced Robotics,* 28**,** 1419-1429.

KLIMCHIK, A., WU, Y., DUMAS, C., CARO, S., FURET, B. & PASHKEVICH, A. Identification of geometrical and elastostatic parameters of heavy industrial robots. Robotics and Automation (ICRA), 2013 IEEE International Conference on, 6-10 May 2013 2013b. 3707-3714.

KÖVECSES, J. & ANGELES, J. 2007. The stiffness matrix in elastically articulated rigid-body systems. *Multibody System Dynamics,* 18**,** 169-184.

MEGGIOLARO, M. A., DUBOWSKY, S. & MAVROIDIS, C. 2005. Geometric and elastic error calibration of a high accuracy patient positioning system. *Mechanism and Machine Theory,* 40**,** 415-427.

PASHKEVICH, A., KLIMCHIK, A., CARO, S. & CHABLAT, D. 2010. Stiffness Modelling of Parallelogram-Based Parallel Manipulators. *In:* PISLA, D., CECCARELLI, M., HUSTY, M. & CORVES, B. (eds.) *New Trends in Mechanism Science.* Springer Netherlands.

PASHKEVICH, A., KLIMCHIK, A. & CHABLAT, D. 2011. Enhanced stiffness modeling of manipulators with passive joints. *Mechanism and machine theory,* 46**,** 662-679.

QUENNOUELLE, C. & GOSSELIN, C. Á. 2008. Stiffness matrix of compliant parallel mechanisms. *Advances in Robot Kinematics: Analysis and Design.* Springer.